

An Edge-Coupled Magnetostatic Bandpass Filter

Connor Devitt, *Graduate Student Member, IEEE*, Renyuan Wang, *Member, IEEE*,
Sudhanshu Tiwari, *Member, IEEE*, Sunil A. Bhave, *Senior Member, IEEE*

Abstract—This paper reports on the design, fabrication, and characterization of an edge-coupled magnetostatic forward volume wave bandpass filter. Using micromachining techniques, the filter is fabricated from a yttrium iron garnet (YIG) film grown on a gadolinium gallium garnet (GGG) substrate with inductive transducers. By adjusting an out-of-plane magnetic field, we demonstrate linear center frequency tuning for a 4th-order filter from 4.5 GHz to 10.1 GHz while retaining a fractional bandwidth of 0.3%, an insertion loss of 6.94 dB, and a -35dB rejection. We characterize the filter nonlinearity in the passband and stopband with IIP3 measurements of -4.85 dBm and 25.84 dBm, respectively. When integrated with a tunable magnetic field, this device is an octave tunable narrowband channel-select filter.

Index Terms—Micromachining, magnetostatic wave (MSW), yttrium iron garnet (YIG), tunable bandpass filter, edge-coupled

I. INTRODUCTION

COUPLED micro-electromechanical resonators with high quality factors (Q-factor) and miniaturized footprints have been an attractive technology for integration in wireless communication systems as narrowband channel-select filters. Wang *et al* [1] has demonstrated high-order micromechanical bandpass filters using one-dimensional (1D) arrays of mechanically-coupled resonators. However, for higher-order filters, long mechanical coupling beams become impractical due to size constraints [2] while sensitivity due to fabrication variation causes increased insertion loss and passband distortion [3]. The high sensitivity of weak electrostatic or mechanical edge-coupled resonators due to structural asymmetries has been leveraged for sensitive parametric mass sensing applications in [2], but prohibits their use in filters. 2D microresonator arrays have shown some success by utilizing weak coupling in one dimension to achieve pass band shape and strong coupling in the other dimension to reduce effects of fabrication variation, but suffer from high insertion loss

Manuscript received on XX XX, 2023; revised on XX XX, 2024; accepted on XX XX, 2024. This research was developed with funding from the Air Force Research Laboratory (AFRL) and the Defense Advanced Research Projects Agency (DARPA). The views, opinions and/or findings expressed are those of the authors and should not be interpreted as representing the official views or policies of the Department of Defense or the U.S. Government. This manuscript is approved for public release; distribution A: distribution unlimited. (*Corresponding authors: Connor Devitt, Renyuan Wang*)

R.W. invented the device concept, and developed baseline model and device design. C.D. performed simulations on fabrication variations and total filter loss, chip fabrication and characterization, as well as data analysis. Manuscript was prepared by C.D. with inputs from R.W., S.T., and S.A.B.

Connor Devitt (e-mail: devitt@purdue.edu), Sudhanshu Tiwari (e-mail: tiwari40@purdue.edu), and Sunil A. Bhave (e-mail: bhave@purdue.edu) are with the OxideMEMS Lab, Elmore Family School of Electrical and Computer Engineering, Purdue University, West Lafayette, IN 47907 USA.

Renyuan Wang is with FAST Labs, BAE Systems, Inc., Nashua, NH 03060 USA (e-mail: renyuan.wang@baesystems.com).

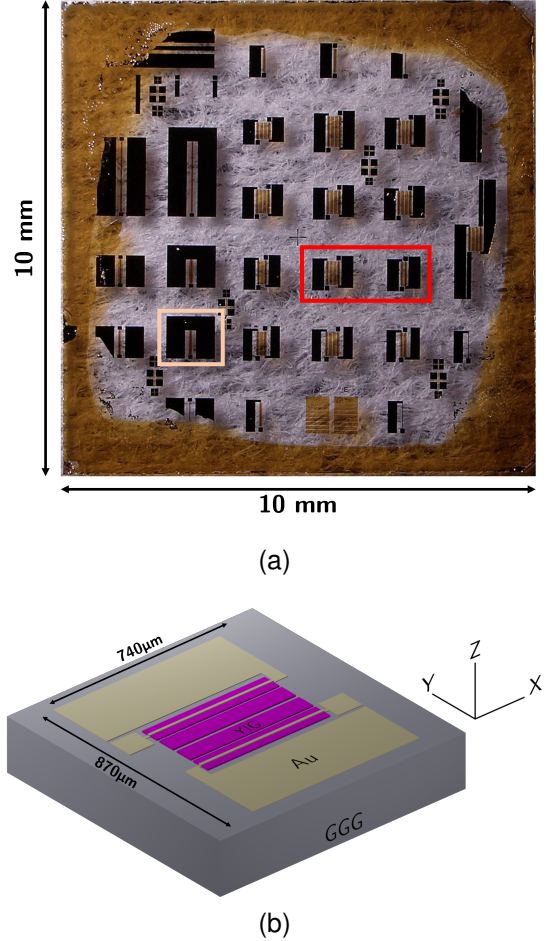


Fig. 1. (a) Chip microphotograph of multiple MSW bandpass filters and 1-port resonators fabricated on a YIG on GGG chip using YIG micromachining technology [6]. A 4-pole filter (on the left) and a 2-pole filter (on the right) are highlighted in red. A 1-port resonator is highlighted in orange. (b) Rendering of a 4-pole bandpass filter featuring four YIG resonators with gold electrodes conformally deposited over the etched YIG. Magnetic bias is oriented out-of-plane along the z -axis.

[3]. Coupled resonator arrays utilizing magnetostatic waves (MSW) have the potential to overcome the weak coupling and extremely narrow bandwidths achieved by electrostatically coupled micromechanical resonators [4], [5] while introducing a degree of tunability.

The magnetostatic wave resonance can be tuned more than an octave in frequency using a static magnetic field ensuring that the filter size does not scale to sub-micrometer dimensions at high-frequencies. Yttrium iron garnet (YIG) is the most widely used material for MSW devices due to its low Gilbert damping ($\alpha = 2.8 \times 10^{-4}$ for a 100 nm film [7]) and experimentally demonstrated Q-factors exceeding 3000 [8], [9]. In state of the art YIG sphere filters [10]–

[12], polished YIG resonators are attached to a thermally conductive rod and manually aligned to non-planar inductive loops acting as transducers. The assembled sphere and loop structures are then coupled through transmission lines similar to the coupling beams in [1] to synthesize a filter. Planar YIG resonators can magnetically couple if they are fabricated in close proximity (Fig. 1b), analogous to the electrically coupled mechanical resonators in [2], [13] or coupled electromagnetic resonators. Magnetically coupled YIG filters can be fabricated at scale using micromachining techniques on films grown on a gadolinium gallium garnet (GGG) substrate, allowing for miniaturization and eliminating the need for polishing and meticulous manual alignment.

II. BANDPASS FILTER DESIGN

The bandpass filter shown in Fig. 1b consists of a number of closely-spaced rectangular YIG magnetostatic forward volume wave (MSFVW) resonators with shorted 300 nm-thick gold inductive transducers conformally deposited over the outermost resonators. With an out-of-plane DC magnetic bias, the RF magnetic field from the transducers excite MSFVW modes in the YIG mesa. Forward volume waves are a family of highly dispersive modes in a thin film whose lowest order mode is described by the dispersion relation [14]:

$$\omega^2 = \omega_0 \left[\omega_0 + \omega_m \left(1 - \frac{1 - e^{-k_{mn}t}}{k_{mn}t} \right) \right], \quad (1)$$

where $\omega_m = \mu_0 \gamma_m M_s$, $\omega_0 = \mu_0 \gamma_m H_{DC}^{eff}$, t is the film thickness, γ_m is the gyromagnetic ratio, μ_0 is the permeability of free space, k_{mn} is the wave vector, M_s is the saturation magnetization, and H_{DC}^{eff} is the effective DC magnetic field. Considering the limits as $k_{mn} \rightarrow 0$ and $k_{mn} \rightarrow \infty$ in the dispersion relation, ω is restricted within the range [14]:

$$\omega_0 \leq \omega \leq \sqrt{\omega_0 (\omega_0 + \omega_m)}, \quad (2)$$

denoted as the spin wave manifold. When the planar dimensions of the thin YIG film are bounded, the magnetostatic waves reflects off the edges forming a standing waves with wave vectors approximately given by [15]–[19]:

$$k_{mn} = \sqrt{\left(\frac{\pi m}{l}\right)^2 + \left(\frac{\pi n}{w}\right)^2}, \quad m, n = 1, 2, 3 \dots \quad (3)$$

where l and w are the length and width of the cavity respectively. These MSFVW resonances can be further understood through an analogy to Lamb waves in a piezoelectric plate [20]–[23]. An oscillating electric field perturbs the polarization of the piezoelectric film generating a stress field and exciting an acoustic wave. In the ferrimagnetic film, an oscillating magnetic field, conversely, perturbs the static magnetization leading to a precession of spins. Both the piezoelectric and magnetostatic cavities support a discrete number modes whose wave vectors depend on the cavity dimensions. Nonlinear dispersion relates the wave vectors to the resonant frequencies for both MSFVW and Lamb waves. For MSFVW, this leads to irregularly spaced modes which all reside in the spin wave manifold.

Unique to MSW, the applied out-of-plane magnetic field shifts the MSFVW dispersion relation in frequency where the tuning rate for the fundamental mode is given by

$$\frac{\partial \omega}{\partial H_{DC}^{eff}} = \mu_0 \gamma_m \frac{2\omega_0 + \omega_m \left(1 - \frac{1 - e^{-k_{mn}t}}{k_{mn}t} \right)}{2\sqrt{\omega_0 \left[\omega_0 + \omega_m \left(1 - \frac{1 - e^{-k_{mn}t}}{k_{mn}t} \right) \right]}}, \quad (4)$$

which simplifies to $\mu_0 \gamma_m = 2.8 \text{ MHz/Oe}$ (for YIG) when $k_{mn}t \ll 1$. The magnetostatic scalar potential, ψ , decays exponentially outside the YIG mesa [14], [24] so the MSFVW resonance in one YIG mesa may couple to adjacent mesas if there is sufficient overlap in their scalar potentials [25]. Consequently, the spacing of adjacent resonators and their vertical sidewall profile are critical to control the inter-resonator coupling strength. For the 4-pole filter in Fig. 1b, the resonator spacings are $s_1 = 10 \mu\text{m}$, $s_2 = 15 \mu\text{m}$, and $s_3 = 10 \mu\text{m}$. Each has length $l = 500 \mu\text{m}$. The outermost resonators have a width $w_{1,4} = 70 \mu\text{m}$ while the inner resonators are slightly narrower at $w_{2,3} = 67 \mu\text{m}$ which was found to marginally improve insertion loss and higher order width mode suppression based on finite element simulation.

Since each resonator length is much shorter than the electromagnetic wavelength over the tuning range, the 4-pole filter can be modeled with the lumped element circuit show in Fig. 2. A Butterworth-Van Dyke circuit [26], [27] is typically used to model an acoustic resonance where the mechanical mode is described by a series R-L-C tank circuit and the transducers introduce a shunt plate capacitance. In the case of magnetic resonators, the transducer introduces a parasitic series inductance and the MSFVW is modeled using a parallel R-L-C tank circuit instead. L_0 and R_0 represent the parasitic inductance and resistivity of the gold electrodes. R_m , C_m , and L_m represent the MSFVW resonance of each YIG mesa. M_{nm} is the inter-resonator coupling between adjacent YIG mesas while M_{IO} represents input/output inductive coupling of the gold electrodes setting the out-of-band rejection level. Similar to a mechanical coupling coefficient, an effective coupling from the electrical to magnetostatic domain can be defined

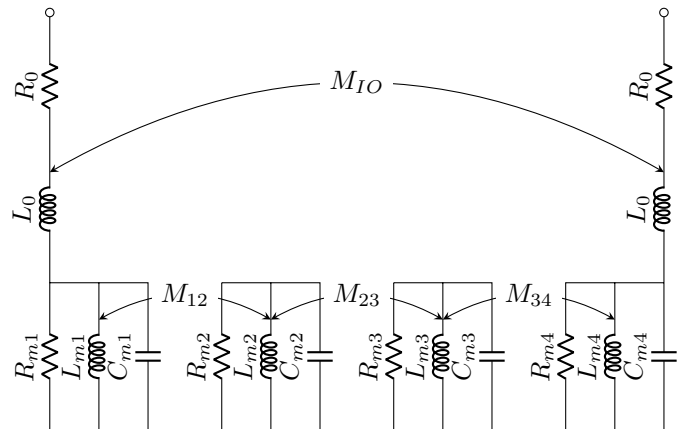


Fig. 2. Lumped circuit model of an edge-coupled 4-pole MSW bandpass filter with electrically short transducers.

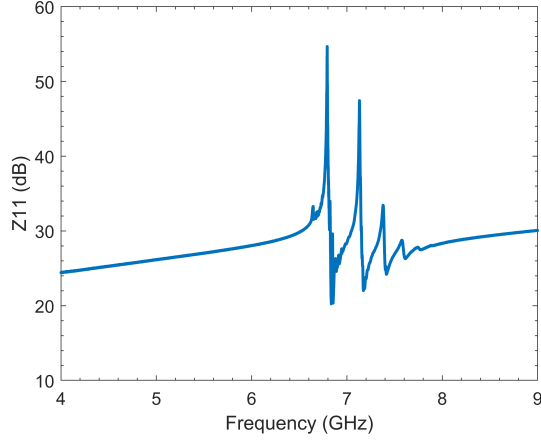


Fig. 3. Measured frequency response of the 1-port resonator highlighted in Fig. 1a at 3962 Oe showing a $Q = 2206$ and $k_{eff}^2 = 1.53\%$.

by (5) where f_p and f_s represents the magnetic resonance and anti-resonance respectively.

$$k_{eff}^2 = \frac{\pi}{2} \left(\frac{f_p}{f_s} \right) \cot \left(\frac{\pi}{2} \frac{f_p}{f_s} \right) \quad (5)$$

k_{eff}^2 is a function of the resonator design determined by the ratio of L_m to L_0 . Similar to an acoustic filter, k_{eff}^2 sets a bound on the maximum achievable filter bandwidth and impacts the passband ripple. The representative 1-port resonator (highlighted in Fig. 1a) exhibits a measured effective coupling and quality-factor of $k_{eff}^2 = 1.53\%$ and $Q = 2206$ at 3962 Oe with frequency response shown in Fig. 3. From the measured resonator impedance response, R_0 , L_0 , R_m , C_m , and L_m can all be extracted through separate fittings near the magnetostatic resonance and outside the spin wave manifold where the resonator behaves as an inductor. Using the same resonator parameters, the measured filter response excluding spurious modes can be fit to the lumped model in Fig. 2 by tuning M_{IO} , M_{12} , and M_{23} under the assumption that each resonator has the same resonant frequency and the filter is symmetric. Fig. 8b shows the frequency response of the lumped model fitted to the measured S21 for a 4-pole filter along with the extracted model parameters.

III. FABRICATION

The fabrication process for the MSW bandpass filter is outlined in Fig 4 where steps (a)-(c) are adapted from [6]. A thick photoresist mask (SPR220-7.0) is patterned onto a 3 μm YIG film grown via liquid phase epitaxially (LPE) on a 500 μm GGG substrate. The YIG film is etched through at a rate of 36 nm/min using an optimized ion milling recipe for vertical sidewalls with sufficient intermittent cooling to prevent burning of the photoresist. Optimized lithography for the thick SPR photoresist is crucial to the filter's final performance since the inter-resonator coupling factors, M_{ij} , are sensitive to the physical separation of the etched YIG. With this process, we are able to fully etch resonator spacings as narrow as 3 μm setting the maximum achievable $M_{ij} \leq 1.37\%$ based on finite element simulation. After etching, the resist is removed and

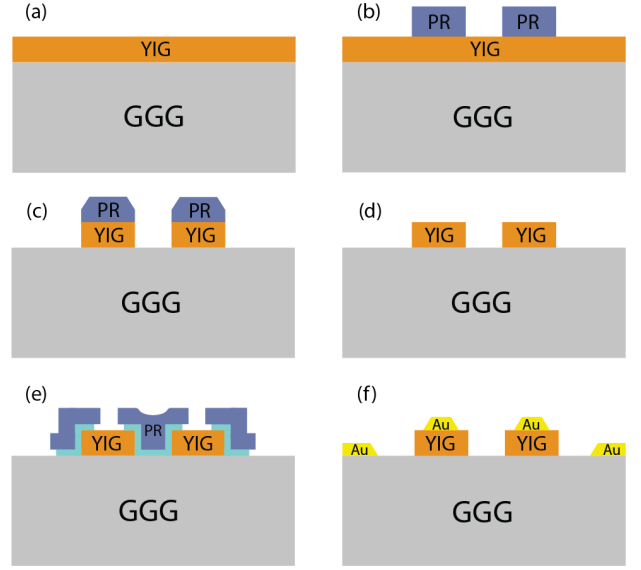


Fig. 4. Fabrication process of the bandpass filter: (a) 3 μm liquid phase epitaxy (LPE) YIG film grown on 500 μm GGG substrate. (b) 7.8 μm thick photoresist (SPR220-7.0) patterned on YIG film as an etch mask. (c) 3 μm ion mill etch of YIG film at a rate of 36 nm/min. (d) Photoresist mask is removed and etched YIG is soaked in phosphoric acid at 80 $^\circ\text{C}$ for 20 min. (e) Bi-layer photoresist (SPR220-7.0 and LOR 3B) mask for a liftoff is patterned onto the etched sample. (f) 10 nm Ti and 300 nm Au is deposited using glancing angle e-beam evaporation followed by a liftoff process.

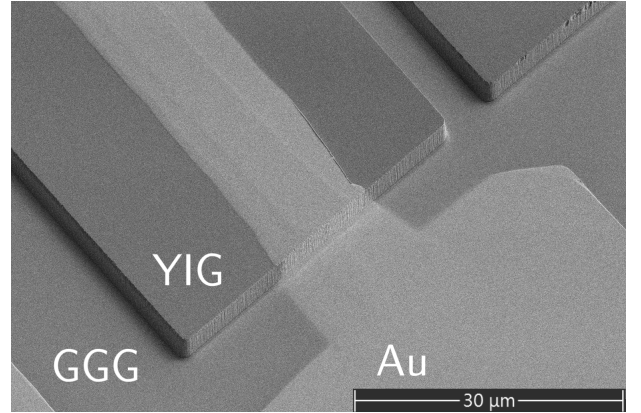


Fig. 5. SEM of the MSFVW bandpass filter showing vertically etched YIG resonators with an inter-resonator spacing of 10.5 μm and conformal gold electrodes over the edges of etched YIG.

the sample is soaked in phosphoric acid at 80 $^\circ\text{C}$ to remove redeposited material. For the gold electrodes, a SPR220-7.0 photoresist mask with a liftoff resist (LOR 3B) bi-layer is patterned for a liftoff process. Using a glancing angle e-beam evaporation, 300 nm of gold and a 10 nm titanium adhesion layer is conformally deposited over the etched YIG resonators. Finally, the sample is soaked in Remover PG overnight to complete the liftoff process. Fig. 5 shows an SEM of a fabricated filter illustrating the vertically etched YIG and conformal gold electrodes. Due to the combination of bi-layer liftoff and angled metal deposition, the gold electrodes are larger than designed and show a tapered thickness.

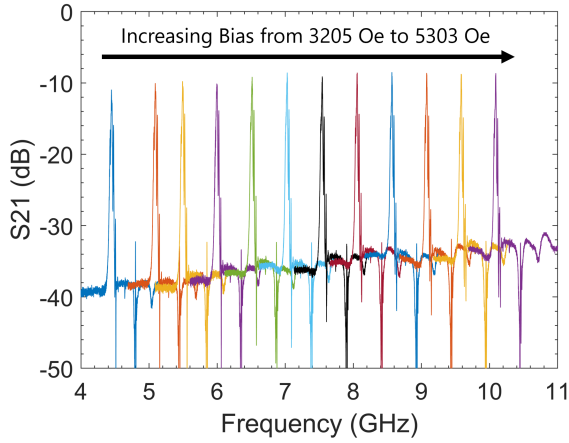


Fig. 6. Measured 4-pole MSW bandpass filter frequency response at different out-of-plane magnetic biases from 3205 Oe to 5303 Oe.

IV. EXPERIMENTAL RESULTS

Filter s-parameters are measured using an Agilent PNA-L N5230A network analyzer with a pair of ground-signal (GS) probes from 3205 Oe to 5303 Oe corresponding to a center frequency tuning over 5.6 GHz as shown in Fig. 6. A single-pole electromagnet powered by a constant current source provides the required out-of-plane magnetic bias (pictured in Fig. 7) and a single-axis Gauss meter is used to map the source current to the applied field. Prior to each measurement, the device under test is aligned to the center of the electromagnet's pole to ensure field uniformity. Fig. 8 shows the frequency response near the passband for a 2-pole and 4-pole filter at 3864 Oe. Outside of the spin wave manifold, no magnetostatic waves may propagate so the filter behaves as two coupled inductors. Consequently, the out-of-band rejection is governed by the inductive coupling strength between the input and output electrodes. For the 2-pole filter with an electrode spacing of $67\ \mu\text{m}$, the rejection is $-25\ \text{dB}$ while for the 4-pole filter with a spacing of $229\ \mu\text{m}$, the rejection is $-35\ \text{dB}$. At 3864 Oe, the 2-pole filter shows an insertion loss (IL) of $-3.55\ \text{dB}$ and a 3 dB bandwidth of 57.0 MHz while the 4-pole filter has an IL of 6.94 dB and a 3 dB bandwidth of 17.0 MHz. From Fig. 8a and 8b, higher-order magnetostatic spurious modes are visible to the right of the passband with a frequency separation of 29 MHz – 40 MHz. As described in [15], the current distribution along the transducer length can excite

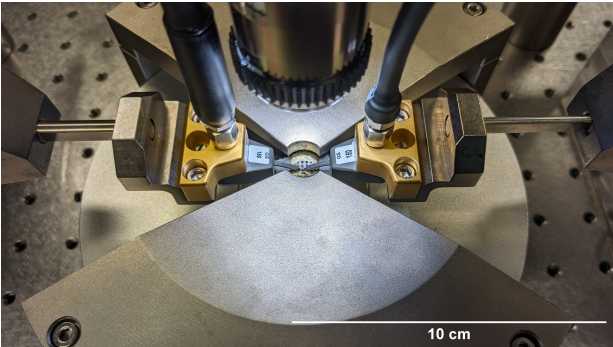
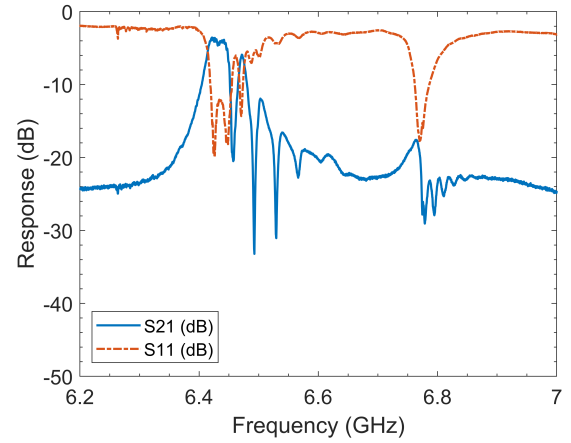
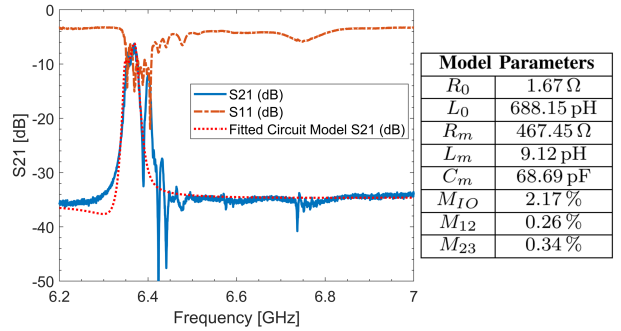


Fig. 7. Experimental setup showing the fabricated filter chip resting on the pole of an electromagnet, two GS probes connected to one device under test, and an optical microscope used for probe landing and device alignment.



(a)



(b)

Fig. 8. Frequency responses for the (a) 2-pole and (b) 4-pole filters highlighted in Fig. 1 near the passband at 3864 Oe. (b) also shows a comparison of the fitted lumped element model in Fig. 2 with measured S21. The fitted circuit assumes all four resonators are identical and excludes the spurious pass bands caused by higher order MSFVW modes.

either even or odd ordered modes. Based on the resonator dimensions and electrically short transducer, the frequency spacing of these spurs agree well with odd ordered length modes. Fig. 9 shows the linear center frequency tuning at a rate of 2.7 MHz/Oe and the 3 dB-bandwidth over the applied bias for the 4-pole filter. With a well-calibrated bias field, the extrapolated center frequency tuning line should intersect $-\omega_m$ at 0 Oe. However, the Gauss meter used for the field

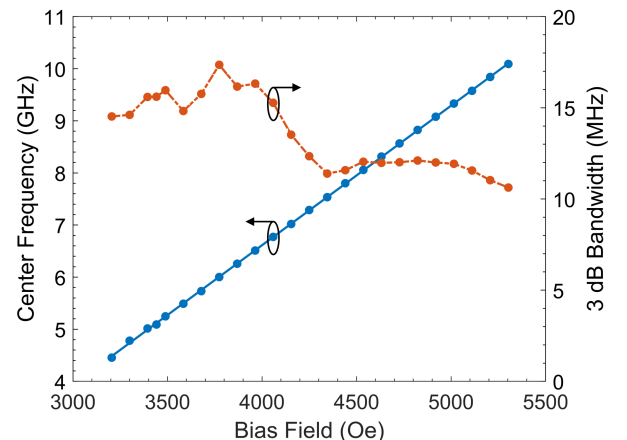


Fig. 9. Measured 3 dB bandwidth and center frequency of the 4-pole MSFVW filter showing a tuning rate of 2.7 MHz/Oe.

calibration is thicker than the fabricated chip, so the reported bias is underestimated by approximately 219 Oe. The filter's tuning was also measured using a neodymium permanent magnet mounted on a 3-axis stage to precisely calibrate the field accounting for any thickness difference between the chip and sensor. In this setup, the extrapolated 0 Oe intersection is at $\omega_m = \mu_0\gamma_m \cdot 1751$ Oe which agrees well the saturation magnetization of LPE YIG.

Considering the total loss $(1 - |S_{11}|^2 - |S_{21}|^2)$ for the 2-pole filter biased at 3652 Oe and measured far away from all magnetostatic resonances, an average of 43% of the input power is dissipated in the thin 300 nm gold transducers, radiated, or absorbed by the YIG on GGG substrate. Based on finite element simulations, the loss is primarily attributed to the resistance of the gold transducers. A second sample was fabricated with 3 μm electroplated gold to reduce resistive losses. Fig. 10 compares the measured insertion loss and total loss for the same 2-pole filter with different gold thicknesses. As expected, the mean out-of-band loss shows significant improvement from 43% to only 12%. The average loss within the 3dB bandwidth exhibits a slight improvement dependent

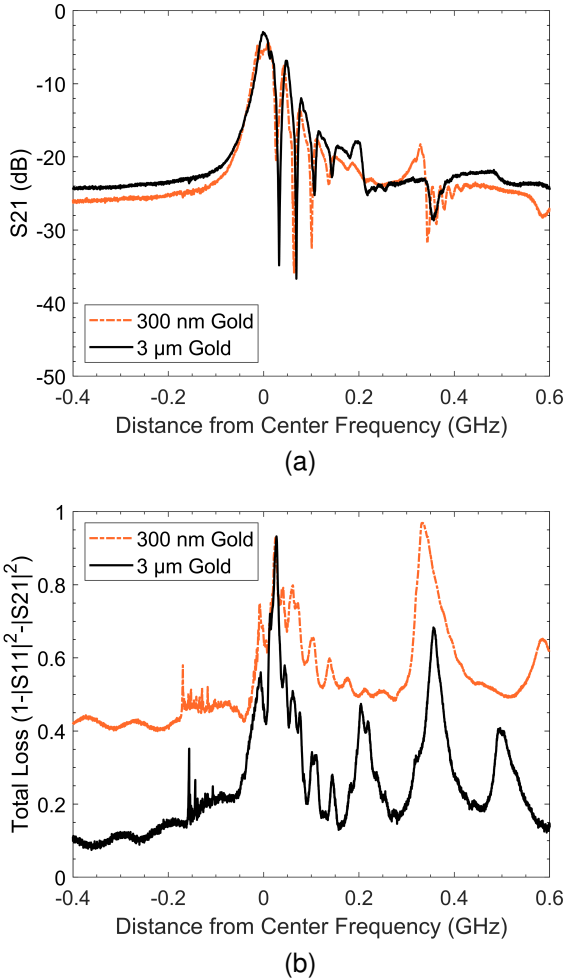


Fig. 10. (a) Measured S_{21} and (b) total loss for 2-pole filters with 300 nm and 3 μm thick gold transducers biased at 3652 Oe and 3660 Oe respectively. Frequency is plotted relative to the center frequency to account for the slight difference in bias strength.

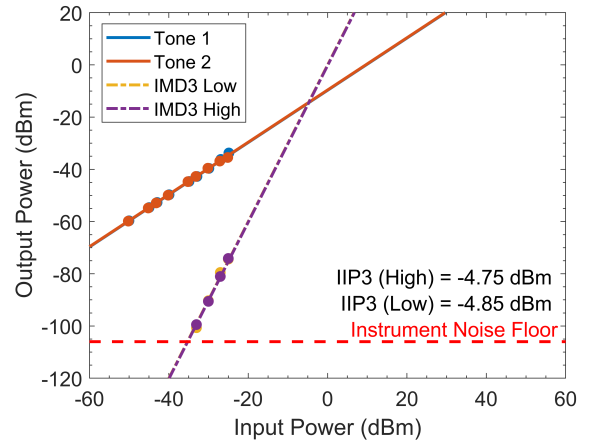


Fig. 11. Two-tone IIP3 measurement in the passband of a 4-pole filter at 3652 Oe bias

TABLE I
UPPER INPUT TONE FREQUENCIES FOR IIP3 MEASUREMENTS

Bias Field	Stopband Low	Passband	Stopband High
3652 Oe	5.465 GHz	5.799 GHz	6.055 GHz

TABLE II
SUMMARY OF 4-POLE FILTER IIP3

Bias Field	Stopband Low	Passband	Stopband High
3652 Oe	≥ 37.95 dBm	-4.85 dBm	25.84 dBm

on bias, ranging from 0.5% to 14.5%. The insertion loss improvement reflects the change in mean in-band loss with a maximum improvement from 4.43 dB to 2.92 dB around 3660 Oe.

The linearity of the MSW bandpass filter is evaluated by measuring the input referred 3rd order intercept point (IIP3) in the passband as well as the stopband both below and above the passband at a bias of 3652 Oe. The nonlinearity measurements are performed using two Keysight E8257D signal generators with a frequency separation of $\Delta f = 15$ MHz. The higher of the two tone frequencies for each region are listed in Table I. A wideband power divider combines the two tones while an Agilent PXA spectrum analyzer measures the resultant spectrum. A two-stage calibration is performed to remove all cable and system losses at every tone frequency and input power level. Far away from the passband, the filter is expected to be linear and no intermodulation products were observed. Based on the maximum output power of the signal generators and noise floor of the spectrum analyzer, the lower stopband IIP3 is estimated to be greater than 37.95 dBm at 3652 Oe. The passband shows the greatest nonlinearity with an IIP3 of -4.75 dBm at 3652 Oe as shown in Fig. 11. The measured IIP3 in each frequency region is summarized in Table II.

V. CONCLUSION

In this paper, we have demonstrated a novel edge-coupled highly-tunable magnetostatic bandpass filter using state-of-the-art micromachining fabrication techniques. The designed 2-pole and 4-pole filters have been tuned over an octave

TABLE III
PERFORMANCE COMPARISON WITH OTHER TUNABLE BANDPASS FILTERS

Reference	Frequency Tuning (GHz)	Insertion Loss (dB)	Bandwidth (MHz)	Rejection (dB)
This work (2-pole)	4.5-10.1	< 6	29-39	> 25
This work (4-pole)	4.5-10.1	< 11	11-17	> 35
YIG Sphere [10]	2-8	< 5	20	> 50
Magnetostatic Surface Wave [28]	3.4-11.1	< 5.1	18-25	> 25
RF MEMS Tunable Filter [29]	6.5-10	< 5.6	306-539	> 50
Evanescent-Mode Cavity [30], [31]	3-6.2	< 4	15-25	> 50

from 4.5 GHz to 10.1 GHz showing a consistent passband shape with performance comparable to other state-of-the-art frequency tunable bandpass filters as summarized in Table III. We have also characterized the linearity of the filter in three distinct frequency regions. Our micromachining process enables precise control over the YIG mesa shape and spacings to synthesize miniaturized MSW channel-select filters analogous to electromagnetic cavity filter design.

DATA AVAILABILITY

The code and data used to produce the plots within this work will be released on the repository Zenodo upon publication.

ACKNOWLEDGMENTS

Chip fabrication was performed at the Birk Nanotechnology Center at Purdue. Resonator and filter measurements and characterization were performed at Seng-Liang Wang Hall at Purdue. The Purdue authors would like to thank Dave Lubelski for assistance with the glancing angle metal deposition and Yiyang Feng for discussions on the fabrication recipes.

REFERENCES

- [1] K. Wang and C.-C. Nguyen, "High-order medium frequency micromechanical electronic filters," *Journal of Microelectromechanical systems*, vol. 8, no. 4, pp. 534–556, 1999.
- [2] P. Thiruvengathanathan, J. Yan, J. Woodhouse *et al.*, "Enhancing parametric sensitivity in electrically coupled mems resonators," *Journal of Microelectromechanical Systems*, vol. 18, no. 5, pp. 1077–1086, 2009.
- [3] D. Weinstein, S. A. Bhave, M. Tada *et al.*, "Mechanical coupling of 2d resonator arrays for mems filter applications," in *2007 IEEE International Frequency Control Symposium Joint with the 21st European Frequency and Time Forum*. IEEE, 2007, pp. 1362–1365.
- [4] S. Pourkamali, R. Abdolvand, G. Ho *et al.*, "Electrostatically coupled micromechanical beam filters," *17th IEEE International Conference on Micro Electro Mechanical Systems. Maastricht MEMS 2004 Technical Digest*, pp. 584–587. [Online]. Available: <http://ieeexplore.ieee.org/document/1290652/>
- [5] A. Alastalo and V. Kaajakari, "Systematic design approach for capacitively coupled microelectromechanical filters," *IEEE Transactions on Ultrasonics, Ferroelectrics and Frequency Control*, vol. 53, no. 9, pp. 1662–1670. [Online]. Available: <http://ieeexplore.ieee.org/document/1678194/>
- [6] Y. Feng, S. Tiwari, S. A. Bhave *et al.*, "Micromachined Tunable Magnetostatic Forward Volume Wave Bandstop Filter," *IEEE Microwave and Wireless Technology Letters*, vol. 33, no. 6, pp. 807–810, Jun. 2023. [Online]. Available: <https://ieeexplore.ieee.org/document/10111074/>

- [7] C. Dubs, O. Surzhenko, R. Linke *et al.*, "Sub-micrometer yttrium iron garnet lpe films with low ferromagnetic resonance losses," *Journal of Physics D: Applied Physics*, vol. 50, no. 20, p. 204005, 2017.
- [8] S. Dai, S. A. Bhave, and R. Wang, "Octave-tunable magnetostatic wave yig resonators on a chip," *IEEE Transactions on Ultrasonics, Ferroelectrics, and Frequency Control*, vol. 67, no. 11, pp. 2454–2460, 2020.
- [9] R. Marcelli, P. De Gasperis, and L. Marescialli, "A tunable, high q magnetostatic volume wave oscillator based on straight edge yig resonators," *IEEE transactions on magnetics*, vol. 27, no. 6, pp. 5477–5479, 1991.
- [10] Micro Lambda Wireless Inc., "MLFD series dual-two." [Online]. Available: <https://www.microlambdawireless.com/uploads/pdfs/MLFD%20Series%20Dual-Two.pdf>
- [11] Teledyne Technologies, "A new approach to yig-based band-reject filters – an introduction." [Online]. Available: <https://www.teledynedefenseelectronics.com/rfµwave/Documents/22-10%20Oct%20-%20Teledyne%20RF&M%20Super%20Band-Reject%20Notch%20Filters%20AN%20v1.02.pdf>
- [12] Micro Lambda Wireless Inc., "Technology description yig tuned filters – an introduction." [Online]. Available: <https://www.microlambdawireless.com/resources/ytfdefinitions2.pdf>
- [13] P. Thiruvengathanathan, J. Yan, J. Woodhouse *et al.*, "Ultrasensitive mode-localized mass sensor with electrically tunable parametric sensitivity," *Applied Physics Letters*, vol. 96, no. 8, p. 081913, 2010.
- [14] D. D. Stancil, *Theory of magnetostatic waves*. Springer Science & Business Media, 2012.
- [15] W. S. Ishak and K.-W. Chang, "Tunable microwave resonators using magnetostatic wave in yig films," *IEEE transactions on microwave theory and techniques*, vol. 34, no. 12, pp. 1383–1393, 1986.
- [16] W. S. Ishak, C. Kok-Wai, W. E. Kunz *et al.*, "Tunable microwave resonators and oscillators using magnetostatic waves," *IEEE transactions on ultrasonics, ferroelectrics, and frequency control*, vol. 35, no. 3, pp. 396–405, 1988.
- [17] S. Hanna and S. Zeroug, "Single and coupled msw resonators for microwave channelizers," *IEEE Transactions on Magnetism*, vol. 24, no. 6, pp. 2808–2810, 1988.
- [18] R. Marcelli, M. Rossi, and P. De Gasperis, "Coupled magnetostatic volume wave straight edge resonators for multipole microwave filtering," *IEEE Transactions on Magnetism*, vol. 31, no. 6, pp. 3476–3478, 1995.
- [19] R. Marcelli, M. Rossi, P. De Gasperis *et al.*, "Magnetostatic wave single and multiple stage resonators," *IEEE Transactions on Magnetism*, vol. 32, no. 5, pp. 4156–4161, 1996.
- [20] R. Wang, S. A. Bhave, and K. Bhattacharjee, "Design and fabrication of s₀ lamb-wave thin-film lithium niobate micromechanical resonators," *Journal of Microelectromechanical Systems*, vol. 24, no. 2, pp. 300–308. [Online]. Available: <http://ieeexplore.ieee.org/document/7005450/>
- [21] K.-y. Hashimoto, *RF bulk acoustic wave filters for communications*. Artech House, 2009.
- [22] G. Esteves, T. R. Young, Z. Tang *et al.*, "Al_{0.68}Sc_{0.32}N lamb wave resonators with electromechanical coupling coefficients near 10.28%," *Applied Physics Letters*, vol. 118, no. 17, p. 171902. [Online]. Available: <https://pubs.aip.org/apl/article/118/17/171902/236115/Al0-68Sc0-32N-Lamb-wave-resonators-with>
- [23] G. Giribaldi, L. Colombo, and M. Rinaldi, "6–20 GHz 30% ScAlN lateral field-excited cross-sectional lamé mode resonators for future mobile RF front ends," *IEEE Transactions on Ultrasonics, Ferroelectrics, and Frequency Control*, vol. 70, no. 10, pp. 1201–1212. [Online]. Available: <https://ieeexplore.ieee.org/document/10243055/>
- [24] Y. Zhang, D. Cai, C. Zhao *et al.*, "Nonreciprocal Isolating Bandpass Filter With Enhanced Isolation Using Metallized Ferrite," *IEEE Transactions on Microwave Theory and Techniques*, vol. 68, no. 12, pp. 5307–5316, Dec. 2020. [Online]. Available: <https://ieeexplore.ieee.org/document/9238458/>
- [25] R. Marcelli and T. Koike, "Micromachined magnetostatic wave coupled resonators," *IEEE transactions on magnetics*, vol. 41, no. 10, pp. 3502–3504, 2005.
- [26] J. D. Larson, P. D. Bradley, S. Wartenberg *et al.*, "Modified butterworth-van dyke circuit for fbar resonators and automated measurement system," in *2000 IEEE ultrasonics symposium. proceedings. an international symposium (Cat. No. 00CH37121)*, vol. 1. IEEE, 2000, pp. 863–868.
- [27] R. Aigner, "Mems in rf filter applications: Thin-film bulk acoustic wave technology," *Sensors Update*, vol. 12, no. 1, pp. 175–210, 2003.
- [28] X. Du, M. H. Idjadi, Y. Ding *et al.*, "Frequency tunable magnetostatic wave filters with zero static power magnetic biasing circuitry." [Online]. Available: <http://arxiv.org/abs/2308.00907>

- [29] K. Entesari and G. Rebeiz, "A differential 4-bit 6.5-10-GHz RF MEMS tunable filter," *IEEE Transactions on Microwave Theory and Techniques*, vol. 53, no. 3, pp. 1103–1110. [Online]. Available: <http://ieeexplore.ieee.org/document/1406317/>
- [30] H. Joshi, "Multi band RF bandpass filter design," ISBN: 978-1-124-15604-0 Publication Title: ProQuest Dissertations and Theses. [Online]. Available: <https://www.proquest.com/dissertations-theses/multi-band-rf-bandpass-filter-design/docview/748222813/se-2>
- [31] H. Joshi, H. H. Sigmarsson, D. Peroulis *et al.*, "Highly loaded evanescent cavities for widely tunable high-q filters," in *2007 IEEE/MTT-S International Microwave Symposium*. IEEE, pp. 2133–2136, ISSN: 0149-645X. [Online]. Available: <http://ieeexplore.ieee.org/document/4264292/>